Biosensors and Bioelectronics 128 (2019) 113–121

Contents lists available at ScienceDirect

Biosensors and Bioelectronics

journal homepage: www.elsevier.com/locate/bios

Portable fluoride-selective electrode as signal transducer for sensitive and selective detection of trace antibiotics in complex samples

Shengfeng Huang[a,b], Ning Gan[a,*], Xinyu Zhang[a], Yongxiang Wu[a], Yong Shao[c], Zhengjin Jiang[b], Qiqin Wang[b,*]

[a] State Key Laboratory Base of Novel Functional Materials and Preparation Science, Faculty of Materials Science and Chemical Engineering, Ningbo University, Ningbo 315211, China
[b] Institute of Pharmaceutical Analysis, College of Pharmacy, Jinan University, Guangzhou 510632, China
[c] College of chemistry and Life Sciences, Zhejiang Normal University, Jinhua 321000, China

ARTICLE INFO

Keywords:
Fluoride-selective electrode aptasensors
Organic small molecular detection
Toehold strand displacement reaction

ABSTRACT

Ion-selective electrodes (ISE) can rapidly, sensitively detect their corresponding ions and are suitable for field testing. However, most ISE methods cannot detect other targets directly which limits their practice application. Herein, we established an aptamer-sensing platform to detect organic small molecule using a portable fluoride-selective electrode (FSE). To achieve the purpose, novel signal tags were fabricated based on nano metal-organic frameworks (NMOF) encapsulating F^- and labeling aptamers. They were then immobilized on one stir-bar. Subsequently, a double stir-bars (bar-a and b) assisted target recycling strategy was designed to convert organic small molecular target to F^- for signal development and amplification. The movement of tags from bar-a to b can be triggered by the analytes. After reaction, the transferred signal tags in bar-b were washed and released F^- which can be measured by FSE for qualification of the target. The assay was evaluated to detect kanamycin or chloramphenicol which was employed as the representatives of organic small molecular with a low detection limit of 0.35 nmol L^{-1} or 0.46 nmol L^{-1}, respectively. Satisfactory performance was observed in complex sample analysis of kanamycin (milk, fish, urine and serum) with a recovery of 91–108% and an RSD ($n = 6$) < 5%. The proposed method broadens the application of traditional FSE to the detection of organic small molecule. And the employment of NMOF which has higher encapsulating capacity of F^- for preparing signal tags can be extended to FSE based aptasensors.

1. Introduction

Point-of-care testing (POCT) methods have attracted increasing attention in on-site monitoring organic residues in biological or food samples owing to its high-speed, efficiency and visualization (Jung et al., 2015; Luppa et al., 2011). Ion-selective electrodes (ISEs) are part of traditional POCT approaches for the determination of ions in biological matrix (Burnett et al., 2000; Lee et al., 2017), because of the merits of simplicity, fast detection and high selectivity for the candidate ions (Jasielec et al., 2018; Papp et al., 2018; Zdrachek and Bakker, 2017). Moreover, the ISE approaches can also cover the drawbacks of some traditional strip paper methods which are usually qualitative or semi-quantitative (Quinn et al., 2016; Vashist et al., 2015). Fluoride-selective electrodes (FSEs) are a well-known ISE and can detect fluoride ions (F^-) rapidly and sensitively in complex samples and possesses detection limits as low as μg L^{-1} (Buhlmann et al., 2001; Ding et al., 2018; Galvis-Sanchez et al., 2015; Gorski et al., 2010; Guinovart et al., 2017; Ortuno et al., 2009; Rodriguez et al., 2018). To the best of our knowledge, there were few reports about detecting small organic molecules using FSE. One of the main obstacles is lacking a signal conversion method to specifically convert the amount of small organic molecules into F^- which could be detected by FSE. Other issues maybe result from the shortage of proper carrier materials for the simultaneous decoration of active substance and affinity recognition ligands to prepare signal probes. Therefore, to make the most of the advantages of the FSE and broaden its practical application in POCT fields, we hope to employ FSE combined with some specific recognition ligands (e.g. aptamer or antibody) to construct a signal transduction strategy for accurate quantification of small organic molecules.

Aptamer is a special type of single stranded DNA/RNA with a certain base sequence, which has been considered as an ideal recognition component to prepare specific probes (Meng et al., 2016; Song et al.,

* Corresponding authors.
E-mail addresses: ganning@nbu.edu.cn (N. Gan), qiqinxtu@163.com (Q. Wang).

https://doi.org/10.1016/j.bios.2018.12.042
Received 10 October 2018; Received in revised form 14 December 2018; Accepted 21 December 2018
Available online 27 December 2018
0956-5663/

2008). In comparison to other recognition ligands, e.g. antibody, aptamer shows distinguished features such as higher physicochemical stability, easy to synthesize in vitro and mass production. Up to now, many aptasensor methods have been reported to detect different types of targets by signal transduction with some photoactive or electroactive materials (Tolle et al., 2015; Yang et al., 2017). However, FSE based aptasensor has never been developed due to the limited availability of suitable carrier materials.

Metal-Organic Frameworks (MOFs), as carrier materials for active substances or ligands, have attracted wide attention in different fields due to ultrahigh porosity, large specific surface area and loading capacity (Zhou and Kitagawa, 2014; Zhou et al., 2012). In particular, nano sized UiO-66-COOH (Zr-based MOFs with carboxyl groups) was reported to be synthetized in an easy and mild way (DeCoste et al., 2015), which possesses high adsorption capacity for F^- in aqueous solution (Massoudinejad et al., 2016; Yang et al., 2016; Zhao et al., 2014). Furthermore, it can be employed to label aptamer as probes and fabricate biosensors for the detection of some of vital biomarker in cell (Chen et al., 2018; Chen et al., 2017). On the basis of the above, nano UiO-66-COOH can be considered as a candidate carrier material to encapsulate F^- and label aptamer simultaneously as signal probes (NMOF-F^-@Apt).

Inspired by the above ideas, FSE based aptasensor with NMOF-F^-@Apt as signal probes has a great potential for detection of small organic molecules. The probes can specifically recognize organic small molecular compound and convert them into F^- signal. However, F^- also widely exists in many samples e.g. water, foodstuff, serum, urines (Lin et al., 2016; Solangi et al., 2009; Tang et al., 2009; Yang et al., 2016; Zhao et al., 2014), it is necessary to avoid the interference of F^- from the sample itself when using an FSE based aptasensor for measurement. Moreover, some signal-amplified strategies must be designed to detect ultra-trace level of target molecules in real samples.

Antibiotic abuse remains a major issue in the world. Although there are many detection methods for antibiotics e.g. HPLC and HPLC-MS (Guillen et al., 2017; Zhou et al., 2017), the specific and on-site detection of antibiotics in biological or food samples is of great significance and a hard challenge (Gai et al., 2017; Rahman, 2018; Ren et al., 2018; Wang et al., 2016a, 2016b). As shown in Scheme 1, an FSE based aptasensor platform using a double stir-bars assisted target recycling system was designed to detect antibiotics, with kanamycin (KANA) as a model analyte. The double stir-bars system consisting of NMOF-F^- aptamer signal probes and portable FSE can realize signal conversion, amplification and avoid matrix interference. The assay was successfully employed to detect KANA and chloramphenicol residues in biological and food samples (milk, fish, urine and serum). Therefore, the FSE based aptasensor showed great potential for rapid, on-site quantitation of antibiotic residues in complex samples. It can also be extended to detect other analytes by simply changing the base sequence of the aptamer.

2. Materials and methods

2.1. Materials and reagents

N,N-dimethylformamide (DMF, 99.9%), terephthalic acid (TPA, 99.9%) were purchased from Sigma-Aldrich Co., Ltd (St Louis, MO, USA); kanamycin (KANA, 99.9%), chloramphenicol (CAP, 99.9%) and other antibiotics (oxytetracycline (OTC), erythromycin (ETC) and penicillin (PEN), streptomycin (STR), ribostamycin (RIB), thiamphenicol (TAP), Florfenicol (FF) and gentamycin (GENT)) were purchased from National Institute for the Control of Pharmaceutical and Biological Products (Beijing, China); Zirconium (IV) chloride ($ZrCl_4$, 99.9%), sodium floride (NaF, ≥99.0%), trichloroethylene phosphate (TCEP, 99.8%) were purchased from Aladdin (Shanghai, China). All other reagents were of analytical grade and used without further purification. Double-distilled water was used in all the experiments. The aptamer sequence of KANA was selected according to the previous literature (Song et al., 2011) and was obtained from Aladdin (Shanghai, China). All DNA oligonucleotides were purchased from Thermo Fisher Scientific (China) Co., Ltd (Shanghai, China) and purified by HPLC. A standard solution with 50 mg mL^{-1} NaF was used for dilution and detection (Lin et al., 2016). Total ionic strength adjustment buffer (TISAB) was prepared according to the previous study (Seo et al., 2016) in the laboratory including 58 mg mL^{-1} of NaCl, 10 mg mL^{-1} of trans-1,2 diaminocyclohexane-N,N,N′,N′-tetra acetic acid monohydrate and 57 μL mL^{-1} of glacial acetic acid. The pH values of TISAB were adjusted between 5.0 with 7% NaOH (w/v). The buffer of phosphate buffered saline (PBS, pH 7.4) was used in most of reactions. The apparatus section was exhibited Supplementary material (SM).

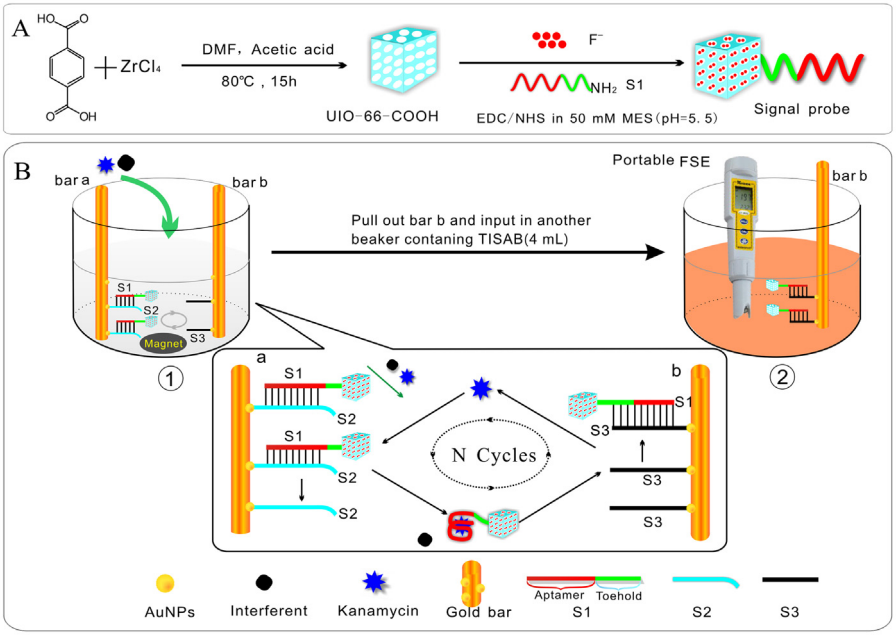

Scheme 1. (A) The preparation procedure of signal probes for FSE based aptasensor; (B) The signal amplification strategy and detection mechanism of antibiotics.

2.2. Synthesis of UiO-66-COOH

UiO-66-COOH was prepared according to the previous report with some modifications (DeCoste et al., 2015; Gan et al., 2016). Typically, $ZrCl_4$ (0.117 g), 1.0 mL of HCl, and 5.0 mL of DMF were added to a 20 mL vial. To dissolve $ZrCl_4$, the vial was subsequently sonicated for 20 min. TPA (0.123 g) and 10 mL DMF were further added to the vial. The final $ZrCl_4$: TPA:HCl:DMF molar ratio was 1:1.5:6:40. The vial was further sonicated until all the TPA was dissolved. Subsequently, the mixture was placed in an autoclave and heated at 80 °C for 15 h. The obtained solid was filtered and washed with DMF twice, and then washed again twice with isopropanol. In the second step, 0.11 g of oxalic acid and the solid obtained in the first step (0.25 g) were dispersed in DMF (50 mL) and subsequently stirred for 2 h at room temperature. The average size of UiO-66-COOH was 112 ± 9.5 nm.

2.3. Preparation of signal probe (NMOF-F⁻@S1)

To synthesize the signal probes, the F^- adsorption experiment was firstly implemented according to the previous study (Lin et al., 2016). 20 mg UiO-66-COOH nanoparticles were dispersed in 5 mL F^- solution (50 mg mL^{-1}) and reacted at room temperature (25 °C) at stirring rate of 300 rpm for 2 h. After being centrifuged at 8000 rpm for 10 min, the resulted precipitation was washed with 20 mL of dual distilled water three times to remove the unspecific adsorptive F^- on NMOF. The obtained NMOF UiO-66-COOH-F^- conjugates (NMOF-F^-) were dispersed and incubated in 500 μL of nucleic acid S1 (10 μM) in 5.0 mL 50 mM 2-morpholino-ethanesulfonic acid buffer (MES, pH = 5.5) at ambient temperature for 4 h. (Gan et al., 2016) Finally, the unspecific adsorbed S1 was removed by washing with 5.0 mL PBS then centrifuging at 8000 rpm for 10 min for 5 times. The signal probes (NMOF-F^-@S1) will be stored in 2.0 mL PBS for further use (Scheme 1-A).

2.4. Fabrication of the double stir-bars assisted target recycling system

AuNPs (about 13 nm in diameter) were prepared via the citrate reduction of $HAuCl_4$ based on this research (Storhoff et al., 1998) with a little bit modification (detailed protocol was exhibited in SM). The obtained AuNPs (100 mg L^{-1}) were subsequently modified on the gold bars (a and b) for 12 h (20 cm in length with diameter of 1 mm to bind aptamer with thiol group according to the report (Wang and Wang, 2004) (Detailed protocol was in SM). Then, the thiol-functionalized DNA (S2) was immobilized on the bar-a@AuNPs through self-assemble protocol. Briefly, 200 μL of S2 (10 μM) was first treated with 1000 μL TCEP (10 mM) for 1 h to cleave the disulfide bond, and then diluted to 5.0 μM with PBS buffer (pH 7.4, 1200 μL). After that, the bar-a modified with AuNPs was immersed in the thiol-functionalized S2 solution overnight at 4 °C. The S2 will be stably labeled on bar-a through Au-S bond to form bar-b@AuNPs-S2. After the bar was washed with 5.0 mL PBS buffer (pH = 7.4) 3 times, it would be dipped into and hybrid with the signal probes solution (2 mL,10 mg mL^{-1} NMOF-F^-@S1 in PBS) at 37 °C for 40 min to consequently form bar-a modified with signal probes. The protocol on modifying the thiol-functionalized S3 (5.0 μM in PBS) on bar-b @AuNPs was the same as that modifying S2 on bar a. Then it was washed with 5.0 mL PBS 3 times to remove the unreacted S3 and bar-b @AuNPs-S3 was successfully synthesized (Scheme 1).

2.5. Determination of antibiotics in complex samples

The detection procedure was illustrated in Scheme 1-B. First, the prepared bar -a and -b were dipped into a plastic vial (No.1) with 4 mL PBS (pH 7.4) and then 40 μL of sample solutions were added. The mixture solutions were gently stirred at 600 rpm (Fig. S-1) for 40 min at ambient temperature. After 40 min, bar-b with signal probes was transferred to another plastic vial (No.2) with 4.0 mL TISAB and stirred for 10 min. Then the released F^- in solution was detected by the portable FSE. The potential responses were employed for quantification of the concentrations of KANA based on a calibration line. The samples pretreatment processes regarding milk, fish, and urine and serum samples were shown in SM.

3. Results and discussion

3.1. The mechanism of the FSE-based aptasensor and double stir-bars assisted target recycling system

The structure of the FSE-based aptasensor, consisting of double stir-bars system and NMOF labeled aptamer probes, was shown in Scheme 1. Kanamycin (KANA) was employed as model analyte to illustrate the strategy. Firstly, the signal probes were prepared by immobilizing S1 covalently (a single-stranded DNA containing KANA aptamer and toehold sequence) on the surface of NMOF-F^-. Meanwhile, bar-a was modified by mercapto S2 (a complementary single-stranded DNA, cDNA of aptamer in S1) and bar-b by mercapto S3 (a complementary single-stranded DNA of S1) base on self-assembly of Au-S bond. Secondly, the signal probes consisting of S1 were hybridized with S2 on bar-a. During the target recycling, the added analyte will preferentially bind with the signal probes on bar-a to form the complex based on the combining of the target with the aptamer sequence in S1. Because the aptamer has higher affinity to the target than to its cDNA, the KANA can replace the cDNA then signal probe-KANA complex will be formed and finally released from bar-a to the supernatant. The probe-KANA complex can subsequently react with S3 on bar-b to form S3-signal probe hybrid and release the target for the next cycle. This is mainly because the binding affinity between S1 and S3 (longer toehold sequence) is greater than that between S1 and KANA. Hence the double stir-bars assisted target recycles can occur and gain signal amplification. Finally, bar b with transferred signal probes was then removed to another vial containing total ionic strength adjustment buffer (TISAB) to elute F^- for FSE measurement. The signal can be employed for quantification of the target. Notably, the procedure on removing bar-b to another vial for F^- measurement can not only avoid matrix interference but also can prevent the interference from endogenous F^- in the samples. As it is well known, FSE was a POCT device (Fig. S-7B) which can detect F^- within half of a minute (Burnett et al., 2000; Lee et al., 2017). Moreover, we employed a portable double stir-bars assisted target recycling system for detection. They were shown in the following Fig. S-7A.

3.2. Characteristics of NMOF, NMOF@ F⁻ and stir-bar

The morphology and structure of the synthesized NMOF (UiO-66-COOH) was characterized by SEM, DSL, EDS and N_2 adsorption-desorption isotherms in Fig. 1. SEM (Fig. 1-A) and DSL (Fig. 1-A) showed that the average size of NMOFs were 112 ± 9.5 nm and well dispersed. The N_2 adsorption-desorption isotherm curve showed the distributions of corresponding pore size of NMOFs were about 1 nm and the surface area of the prepared NMOF was 892.5 m^2 g^{-1} (Fig. 1-B). This means a high encapsulating capacity of F^-.

The EDS experiments were also employed to evaluate if F^- was absorbed in NMOF. As depicted in Fig. 1(C&D), F^- element was not observed in the blank NMOF (Fig. 1-C), while the weight ratio and atom level of F element in the NMOF-F^- probes were calculated as 1.69% and 2.03%, respectively (Fig. 1-D). Furthermore, the XRD spectrum of NMOF-F^- probes before and after immersing in water didn't change, which suggested the probes were very stable in aqueous solution (Fig. S-2). We also calculated the saturated absorption amount of F^- in NMOF-F^- by the formula: absorption amount = $([F^-]_0-[F^-]_t) \times V/m$. V is the total volume of the reaction system, m is the weight of NMOF, $[F^-]_0$ and $[F^-]_t$ was defined as the initial and final concentration of F^- in supernatant, respectively. The saturated adsorption value of NMOF to F^- was calculated as 42 mg g^{-1}. All these results demonstrated that the

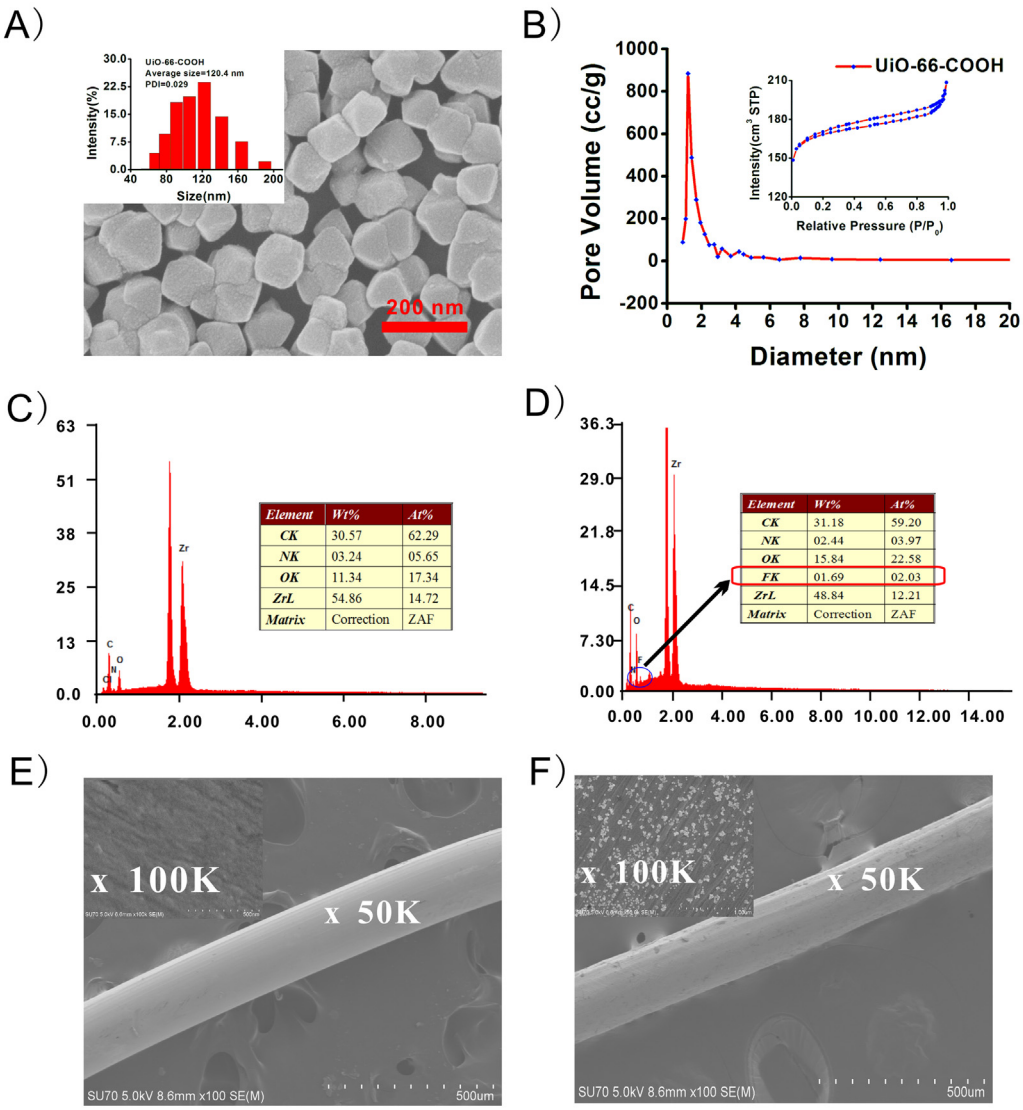

Fig. 1. SEM spectrum and DLS (insert figure) of the prepared nano NMOF (A); N_2 adsorption isotherm curves (B), EDS results of the blank NMOF and the NMOF@ F^-, respectively (C&D); The SEM morphology of bare bar-a (E) the signal probes modified bar-a (F).

NMOF was successfully prepared and was suitable for adsorption F^- to construct fluoride encapsulated signal probes. In addition, the BET spectrum was employed to compare the specific surface area of the UiO-66-COOH and the UiO-66-COOH-F^- to further verify the successful encapsulation of the NMOF-F^- complex. The results were showed in Fig. S-8, which showed that the specific area decreased from 892.5 $m^2\ g^{-1}$ to 564.2 $m^2\ g^{-1}$ after UiO-66-COOH was encapsulated with F^-. The results meant that F^- maybe intercalated into the cavities of the NMOF.

In order to increase the amount of signal probes on bar-a for target recycling, AuNPs were modified on bar-a and -b to increase their specific area. To further confirm the desired results, UV–Vis absorption spectrometry was employed to characterize the conjugation of ssDNA on AuNPs. As shown in Fig. S-3, the characteristic UV peak at 257 nm of DNA was observed on the ssDNA functionalized bare gold bar and bar-a@AuNPs. Moreover, the larger decrease value of ssDNA (S2)'s UV absorption intensity (about 3.5 folds, 400 nmol) was achieved on the bar-a@Au NPs than bare bar-a, which proved that the amount of S2 immobilized on the surface of the bar-a@AuNPs was more than that on bare gold bar. The aptamer hybrid efficiency of S1 with S2 on bar-a@AuNPs can also be measured by UV–Vis absorption spectrometry. The hybrid amount of S1 on bar-a@AuNPs-S2 was about 320 nmol. We also determined the labeling amount of S3 on bar-b@AuNPs was about 420 nmol (300 nmol in pure bar-b). Hence, bar-a and -b modified with AuNPs can greatly increase the amount of immobilized signal probes comparing with the bare gold bar, which is beneficial for the further signal amplification. From the comparison of Fig. 1-E and Fig. 1-F, many AuNPs were modified on bar-a. Furthermore, the calculated results showed that the number of signal probes modified on the gold bar is about 1.03×10^{14} (Detailed protocols and calculation were exhibited in the SM, Tables S-5 and S-6).

3.3. Optimization of the length of the DNA sequence

To verify whether the double stir-bars based toehold-mediated target recycling signal amplification reaction can be established, the DNA sequences in probes were optimized by various combinations of S1, S2, S3 and KANA. As it can be seen in Fig. 2-A, Lane 1 and 2 represent S1 (0.2 μM) with KANA aptamer sequence and S2 (0.3 μM), respectively. Lane 3 represents the hybrid of S1 and S2 (excessive S2 hybrid with S1 to ensure the full combination). It can be seen that an obvious band representing S2/S3 hybrid chains at 65 bps formed and some S2 residues remained. Lane 4 represents the reaction between S1/S2 and KANA (50 nM). The results showed that there were three bands from top to bottom in Lane 4. The band of S1/S2 at the top became

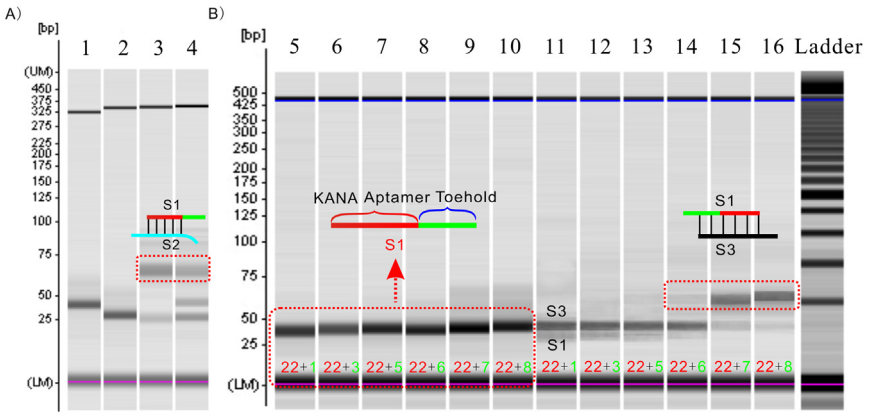

Fig. 2. Verification of reaction between KANA and S1/S2 hybrid (A); and the optimization experiments of toehold base length between S1 and S3 (B).

bleached, while S1 band reappeared and S2 became darker. All these demonstrated that 50 nM KANA can hybrid with the S1 (with aptamer and toehold sequence) and then released S2 from S1/S2. All above results illustrated that the affinity between KANA and S1 with aptamer sequence is stronger than that of S1/S2. Moreover, the replacement of signal probes by KANA from S2/signal probe on bar-a can be realized successfully.

To further investigate the suitable toehold number on S1, different toeholds were designed due to the number of toeholds that can greatly influence the efficiency of target recycling. All the sequences involved in the optimal experiments were listed in Table S-1. S2 (0.3 μM) with different toehold numbers 1, 3, 5, 6, 7 and 8; (red chain represents the base number of aptamer sequences, while the green is the number of toehold chains) designed from lane 5–10 (Fig. 2) to react with KANA. Lane 11–16 represented the reaction between S1/KANA (50 nM) and S3 (300 nM) containing different toehold numbers. It can be found that there was no hybrid band between S1 and S3 (S1/S2) when the toehold number was 1, 3, 5, respectively, then S1 and S3 were separated. There was a light S1/S3 hybrid band shown when the toehold number was 6 (Lane 14). When the toehold number reached to 7, the color of S1/S3 band became darker (Lane 15) than that of Lane 14. And the darkness remained almost the same as Lane 15 when the toehold number reached to 8 (Lane 16). All these results meant the toehold number can obviously influence the efficiency of toehold mediated target recycling. Considering the optimal replacement efficiency and reducing the preparing cost of signal probes, the toehold length of 7 was chosen as the optimal hybrid length for subsequent experiments.

3.4. Optimization of experimental conditions

Some reaction conditions must be optimized, including the elution time of NMOF-F^-@Apt by TISAB, reaction time and temperature for double stir-bars recycling system, to gain the best measurement performance. Insufficient elution time can reduce the detection signal and affect the detection sensitivity. As shown in Fig. 3-A, the potential of F^- increased as elution time increased then reached to the maximum value at 10 min. The recycling time for the antibiotics to react between double stir-bars is another vital parameter to increase the signal-amplified folds of the aptasensor. Fig. 3-B displayed the potential behavior of the aptasensor in KANA (5.0 nM). The potential responses increased gradually with the extended reaction time, and reached the maximum value after 40 min Fig. 3-C showed the signal of KANA at different reaction temperatures. The height of the histogram represented the difference values between the sample and blank signal. With the temperature increasing, the difference value increased simultaneously and achieved the maximum temperature from 25–40 °C. All these meant that room temperature can be selected for further studies. Above all, 10 min of elution time and 40 min reaction time at ambient temperature were chosen in the following experiments.

3.5. Interference from endogenous F^-

In order to further verify whether the proposed method can avoid the interference of endogenous F^- in sample, confirmation experiments were executed. The tap water (TW), milk (Purchased in local market), urine and serum (provided from medical school of Ningbo university. The treatment of all the samples was strictly in compliance with the medical ethics of Ningbo university) were selected as typical samples due to both TW and milk containing F^- (Lin et al., 2016; Massoudinejad et al., 2016). As seen in Fig. 3-D, there is no change of potential signals in the above samples. And the value was close to the fluoride-free solution (−380 mV). We further designed the F^- spiked (10 mM, 100 mM) TW, milk, urine and serum samples and there were also no obvious signal changes. The reasons may be due to that no F^- can pass through the aptamer shell and F ions have been saturated in the signal probes. Finally, 100 nM KANA was spiked in the real samples, and the potential signals were increased dramatically to −354 mV. All these meant the endogenous F^- in samples will not interfere with the detection effect of the aptasensor.

3.6. The elution of F^- from signal probes by different reagents

One important issue for the assay is to investigate the elution conditions of the signal probe, a series of elution experiments were performed using different buffers. As shown in Fig. 4-A, the potential signal of F^- in pure was basically near to blank in PBS and TISAB because there was no F^- inside. The signal F^- from NMOF-F^- washed by PBS and 150 mM Cl^- (both at pH 7.4) was also the same and the signals of F^- were much larger than NMOF, which meant that PBS and Cl^- could wash away the F^- from NMOF-F^-. We found NMOF-F^- was stable and leaking very few F^- in 10 mM Na_2HPO_4 solution existing in PBS. Because PBS also contains about 150 mM Cl^-, these mean that F^- was replaced by Cl^- through ion exchange (Meenakshi and Viswanathan, 2007). When NMOF-F^- was labeled with aptamer to form NMOF-F^-@Apt signal probes and washed by PBS and 150 mM Cl^- (both at pH = 7.4), the F^- signal greatly reduced and was close to pure NMOF. All these meant that F^- in NMOF-F^-@Apt cannot be washed out from them. We measured the zeta potentials of NMOF, NMOF-F^- and NMOF-F^-@Apt (Fig. S-4). The potential was −7.0 mV for NMOF, −13.5 mV for NMOF-F^- and −17.4 mV for NMOF-F^-@Apt. The lower potential of NMOF-F^-@Apt signal probes than NMOF-F^- and NMOF meant there were more negative charges on it. The reason was because large amounts of aptamer with negative charges were modified on NMOF-F^-. As a result, Cl^- is not easily passed through the aptamer shell into the NMOF-F^- core component to replace F^-. That is why the signal probes can remain stable in PBS and the encapsulated F^- can't be washed by

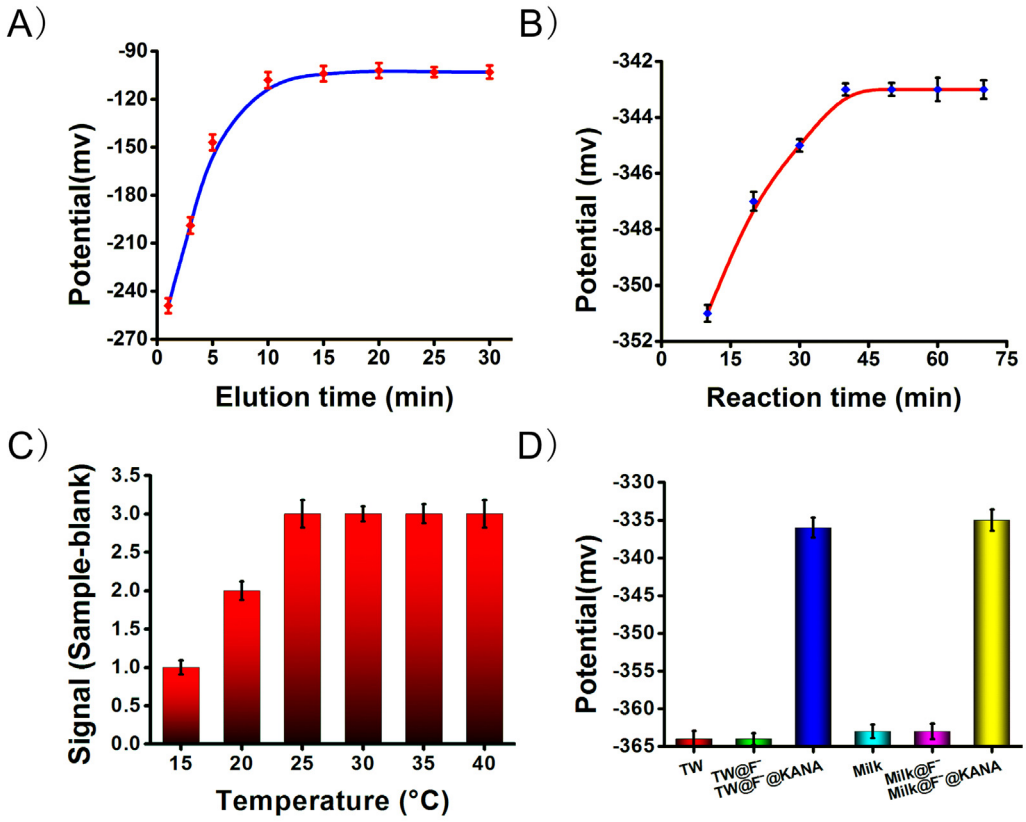

Fig. 3. Optimization of the reaction time of the antibiotics detection system (A); Optimization of the elution time of TISAB (pH = 5.0) for NMOF@F⁻ (B); Optimization of the reaction temperature of the antibiotics detection system (C); the investigation of the matrix interference (D). The entire detection environment was carried out in the TISAB (pH = 5.0) at room temperature.

PBS or Cl^-. All these enabled the reactions done in PBS. However, the F^- signal was the highest from NMOF-F^-@Apt washed by TISAB. We also measured that the zeta potential of NMOF-F^-@Apt was −12.5 mV at TISAB (pH 5.0) because the negative charges of aptamer decreased with pH. These ensured the Cl^- (TISAB contains 58 mg mL^{-1} of NaCl.) in TISAB can pass through the aptamer layer (shell) to replace F^-. We calculated the elution amount of F^- from NMOF-F^-@Apt was 41.5 mg g^{-1} which was the same as NMOF-F^- (42 mg g^{-1}). These results demonstrated that all F^- can be completely washed out by TISAB for signal development. Based on these phenomena, TISAB was employed to wash F^- after the double stir-bars assisted recycling reaction, and PBS was employed for reaction.

3.7. The signal amplification effect of the assay

Fig. 4-B exhibited the signal amplified effect in detection system. It can be seen that in the absence of KANA (Fig. 4-B-a), the signal is close to −360 mv. In the presence of KANA (20.0 nM), only bar-a was used to react with KANA. The potential signal increased to −355 mv (Fig. 4-B-b). The change was very faint. However, when the double stir-bars assisted toehold-mediated target recycling was introduced to react with 20.0 nM KANA (Fig. 4-B-c), the potential value decreased obviously to −331 mv. From the calibration line between potential to pF^-, 8 times the amount of F^- can be detected in the double stir-bars system compared with the unamplified one. The double stir-bars assisted signal amplification can significantly improve the sensitivity. Additionally, the length of the gold bar was optimized based on the reused times and the actual experimental cost. The results (Fig. S-9) showed that the gold bars with 20 cm in length can reach to a plateau. After that, the sensitivity showed limited enhancement and the longer bar have not significant effect for sensitivity. Because the specificity of the sensor depends on the aptamer probes on the stirring bars, the length of gold bar

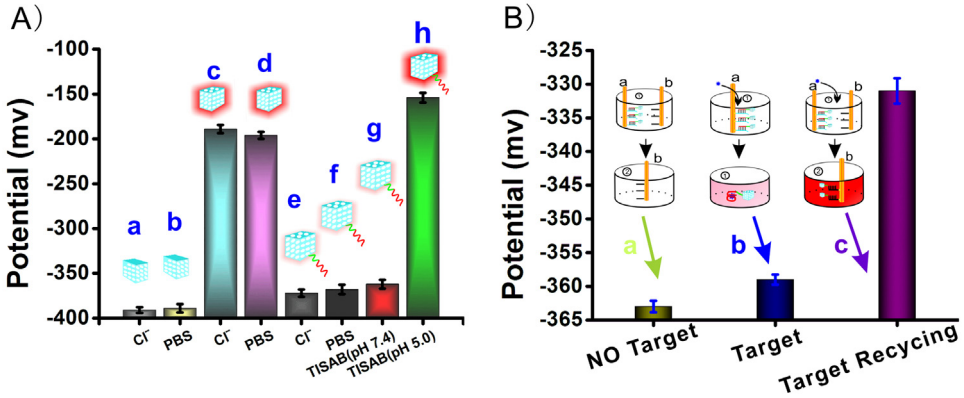

Fig. 4. Investigation of washing effects from the signal probes by different reagents (A), the signal amplification effects based on double stir-bars assisted recycling system (B). The concentration of KANA was 20 nM, and the entire detection environment was carried out in the TISAB (pH = 5.0) at room temperature.

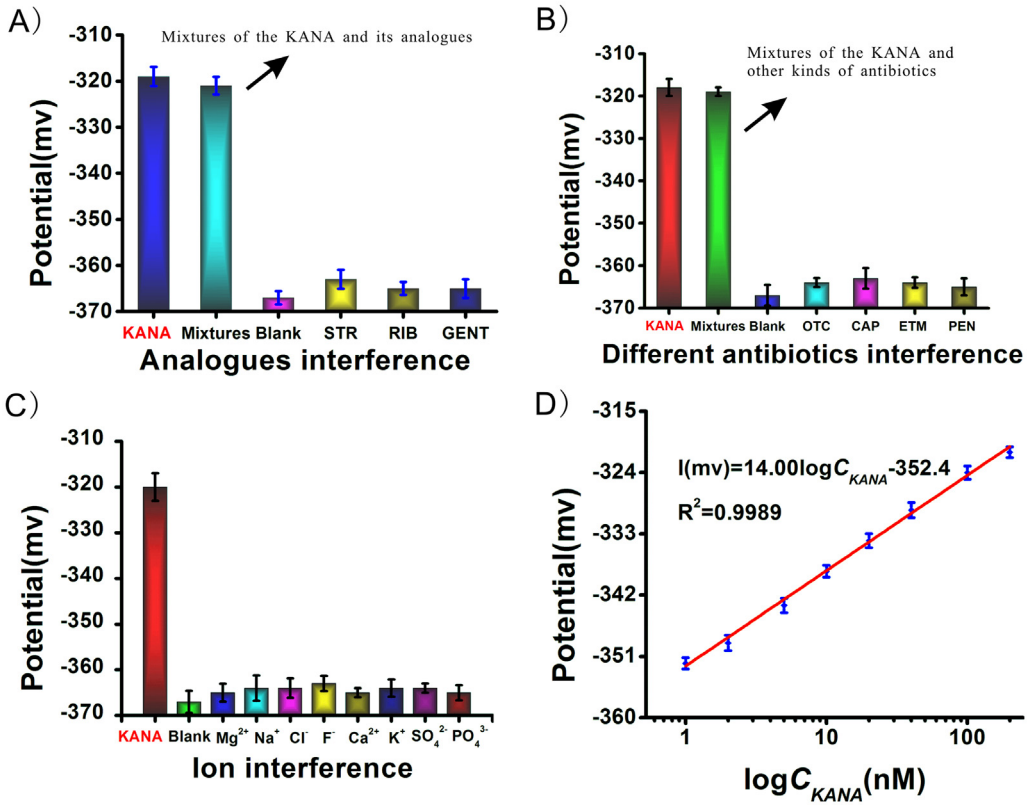

Fig. 5. Selectivity experiments for KANA against other analogues, including STR, RIB, GENT and their mixtures (A); selectivity experiments for KANA against other antibiotics, including OTC, CAP, ETM, PEN (100 nM) and their mixtures (B); the KANA signal against potential coexisting ions (100 mM) in the matrix (C); the calibration plot in the presence of different logarithms concentrations of KANA (D). The concentration of KANA was 50 nM, and the entire detection environment was carried out in the TISAB (pH = 5.0) at room temperature.

can't influence the specificity. We also measured the reusability of stir bar. The longer gold bars can provide more sites for immobilizing more aptamer probes, thus the stir bar can be reused for more times. We found the stir bar with 20 cm can be reused for at least 25 times detection. This proved the stir bar with 20 cm length can immobilize enough probes for detection. Therefore, according to the actual detection effects and in order to avoiding the waste of gold wires, the gold bar with 20 cm was chosen in this experiment.

3.8. The selectivity and crosstalk evaluation

Firstly, KANA with its analogues (aminoglycoside antibiotics: STR, RIB or GENT) and their mixture were selected to validate the selectivity and specificity of the proposed sensor. As it can be seen in Fig. 5-A, the potential value of analogue antibiotics (between −364 and −365 mV) were almost as same as that of blank (−365 mV). While the potential value of KANA (−318 mV) and that of the mixture (KANA mixed with other antibiotic, −321 mV) exhibited almost the same value. These results proved the analogues don't interfere with the detection of KANA while using KANA probes. Furthermore, as shown in Fig. 5-B, good selectivity and specificity of the proposed sensor were also evidenced by employing several other kinds of representative antibiotics, (tetracycline antibiotics OTC, amphenicol antibiotics CAP, macrocyclic antibiotics ETM or antibiotics PEN) and their mixture as analytes. We also testify if there was cross-talking for CAP probes using the same detection platform. Different antibiotics were selected as interfering substances, including CAP's analogues (TAP, FF) and other kinds of antibiotics (OTC, KANA, ETM, PEN) As shown in Table S-7, the potential of CAP (−318 mV) and the mixture (CAP with the interfering antibiotics, −322 mV) were almost same, while the signal of analogues antibiotics and other kinds of antibiotics was as same as the blank (−365 mV). These results indicated that this biosensing method can differentiate multiple antibiotics in a sample and have not potential crosstalk for multiple target antibiotics, including its analogues. In addition, we further investigated the potential interference from other coexisting substances (10 mM carbamide, trioxypurine; 100 mM K^+, Na^+, Ca^{2+}, SO_4^{2-} PO_4^{3-}) to assess the specificity. The results indicated that the coexisting substances had little influence (< 5.0% versus the blank signal) on the detection (Fig. 5-C). All results demonstrated that the system possessed good ability to resist matrix interference. The reasons were as the following: after the double stir-bars assisted recycling reaction, the bar b with signal probes was transferred to another pure reaction system only containing TISAB and no matrix in samples were transferred. Thus, the matrix influences were eliminated.

3.9. The analytical performance of the assay

The linear curve for logarithms concentrations of KANA fitted a regression equation of I (mv) = 14.00 log C_{KANA} − 352.4 (I represents the potential of F^-, and C_{KANA} is the final concentration of KANA) with a correlation coefficient R^2 = 0.9989 (Fig. 5-D). The detection range for KANA was 1.0 ~200 nM with detection limits of 0.35 nmol L^{-1} (S/N = 3), which was competitive or better than other reported single analyte detention assays including other electrochemical, florescence aptasensors (Table S-8) (Blanchaert et al., 2013; El-Attug et al., 2011; Qin et al., 2017; Ramezani et al., 2016; Sharma et al., 2017; C.S. Wang et al., 2016; X.Z. Wang et al., 2016). The good performance and high sensitivity of the aptasensor were attributed to following features the usage of sensitive FSE as detector; high adsorption capacity of F^- in NMOF and the double stir-bars assisted toehold-mediated target recycling for amplification. Moreover, portable FSE as transducer of the aptasensor can obviously reduce the size of detection system and meet the requirement of POCT. All these made it promising for practical and convenient application in the detection of antibiotics in complex samples.

We continuously detected 10 samples (10 mL) with 50 nM KANA by the aptasensor, for investigate the reproducibility of the proposed assay. The signals maintained 90% of the original one. These meant there were too many signals probes in the bars which can enable adequate response efficiency, and the reproducibility was good. Moreover,

Table 1
Detection of KANA in different samples ($\bar{x} \pm s$, n = 6).

Samples	Blank (nM)	Added (nM)	Found (nM)	Recovery (%)	ELISA (nM)
Water-1	/	10.0	10.6 ± 0.13	106	/
Water-2	0.21 ± 0.02	10.0	10.7 ± 0.34	108	/
Water-3	/	20.0	21.2 ± 0.52	106	19.3 ± 1.31
Milk-1	/	5.000	5.26 ± 0.21	105	/
		50.00	47.7 ± 0.71	95.4	49 ± 1.21
Milk-2	/	5.000	4.81 ± 0.17	96.2	/
		50.00	51.6 ± 0.62	103	48.4 ± 2.3
Milk-3	0.43 ± 0.02	5.0	4.59 ± 0.76	91.8	/
		50	49.1 ± 0.23	98.2	51.0 ± 3.1
Fish-1	/	5.0	5.02 ± 0.23	100	/
		50	49.7 ± 0.39	99.4	51.2 ± 1.9
Fish-2	/	5.0	5.12 ± 0.54	102	/
		50	47.7 ± 0.86	95.4	50.9 ± 1.8
Serum	/	5.0	5.30 ± 0.21	106	/
Urine	0.12 ± 0.02	0.20	0.32 ± 0.07	102	/

three levels of KANA (2.0, 5.0 and 50 nM) were used for five replicate measurements to evaluate the intra-day precision, and the inter-day precision of the assay. As listed in Table S-9, the relative standard deviations (RSDs) of intra-day were 0.16%, 0.26% and 0.51% for three levels of KANA, respectively, which indicated an acceptable precision and reproducibility for this method. The RSDs of inter-day were 0.18%, 0.32% and 0.98% for different concentration of KANA, respectively. These results showed a good repeatability. Additionally, the stability of the aptasensor was estimated after being stored at 4 ˚C. There was no obvious change after the aptasensor was stored and the signal decreased only 5% after 3 months. Therefore, the aptasensor exhibited a high degree of high stability for antibiotics detection.

3.10. Application of the aptasensor for detection of KANA in complex samples

To evaluate the analytical effects of the proposed assay in complex samples, the primary and spiked (5.0 and 50.0 nM KANA) milk, fish, urine and serum samples were employed to analyze the target by the proposed method. As shown in Table 1, an acceptable accuracy of KANA detection in the four kinds of samples was obtained with the spiked recoveries from 91.8% to 108%. Good precision was also obtained by assaying relative standard deviation (RSD) via experiments for three times and the RSD values ranged from 0.23% to 1.33%.

3.11. Fabrication of aptasensor for chloramphenicol detection

In addition, we also fabricated an aptasensor to detect CAP by the same principle to further verify the general applicability of the above double stir-bars assisted target recycling and signal conversion strategy. The sequences of S1, S2 and S3 were shown in SM (Table S-2). The results exhibited the established FSE-based aptasensor can detect as low as 0.46 nmol L^{-1} CAP with satisfactory performance in terms of accuracy range from 93% to 104% (Table S-10, Fig. S-6), which demonstrated that the proposed assay is a universal platform for antibiotic detection.

4. Conclusions

In this study, a novel FSE-POCT method based double stir-bars assisted toehold-mediated target recycling strategy was developed for quantification of organic small molecular analyte (such as KANA or CAP) in real samples. Using the specially designed signal probes (NMOF-F^-@Apt) based on nano UiO-66-COOH with encapsulated F^-, the FSE can indirectly detect organic small molecular analyte. A double stir-bar assisted toehold-mediated target recycling strategy was designed for signal amplification and matrix interference avoidance, which can gain 8 fold enhancement of sensitivity. However, the application of the FSE-POCT method should be extended in the future work. More antibiotics and other small organic molecules should be employed to verify the developed assay. Furthermore, some portable, low-cost and robust analytical strategies will be developed for other small organic molecules in complex samples.

CRediT authorship contribution statement

Shengfeng Huang: Writing - original draft, Visualization, Investigation, Conceptualization, Writing - review & editing, Methodology, Data curation. **Ning Gan:** Supervision, Data curation, Conceptualization, Writing - original draft, Validation, Writing - review & editing. **Xinyu Zhang:** Methodology, Data curation. **Yongxiang Wu:** Software, Writing - review & editing. **Yong Shao:** Writing - review & editing. **Zhengjin Jiang:** Writing - review & editing. **Qiqin Wang:** Writing - review & editing, Validation, Supervision.

Acknowledgments

This work was supported by the National Natural Science Foundation of China (No. 11832013), the Natural Science Foundation of Zhejiang Province (LY19B050001, Y18B070008), the Natural Science Foundation of Ningbo (2018A610221) and the K.C. Wong Magna Fund in Ningbo University.

Declaration of interests

None.

Appendix A. Supplementary material

Supplementary data associated with this article can be found in the online version at doi:10.1016/j.bios.2018.12.042.

References

Blanchaert, B., Jorge, E.P., Jankovics, P., Adams, E., Van Schepdael, A., 2013. Chromatographia 76, 1505–1512.
Buhlmann, P., Hayakawa, M., Ohshiro, T., Amemiya, S., Umezawa, Y., 2001. Anal. Chem. 73, 3199–3205.
Burnett, R.W., Covington, A.K., Fogh-Andersen, N., Kulpmann, W.R., Lewenstam, A., Maas, A.H.J., Muller-Plathe, O., Sachs, C., Siggaard-Andersen, O., VanKessel, A.L., Zijlstra, W.G., 2000. Clin. Chem. Lab. Med. 38, 1065–1071.
Chen, W.H., Sung, S.Y., Fadeev, M., Cecconello, A., Nechushtai, R., Willner, I., 2018. Nanoscale 10, 4650–4657.
Chen, W.H., Yu, X., Liao, W.C., Sohn, Y.S., Cecconello, A., Kozell, A., Nechushtai, R., Willner, I., 2017. Adv. Funct. Mater. 27, 1–6.
DeCoste, J.B., Demasky, T.J., Katz, M.J., Farha, O.K., Hupp, J.T., 2015. New. J. Chem. 39, 2396–2399.
Ding, J.W., Yu, N.N., Wang, X.D., Qin, W., 2018. Anal. Chem. 90, 1734–1739.
El-Attug, M.N., Adams, E., Hoogmartens, J., Van Schepdael, A., 2011. J. Sep. Sci. 34, 2448–2454.
Gai, P.P., Gu, C.C., Hou, T., Li, F., 2017. Anal. Chem. 89, 2163–2169.
Galvis-Sanchez, A.C., Santos, J.R., Rangel, A.O.S.S., 2015. Talanta 133, 1–6.
Gan, N., Multia, E., Siren, H., Ruuth, M., Oorni, K., Maier, N.M., Jauhiainen, M., Kemell, M., Riekkola, M.L., 2016. Anal. Biochem. 514, 12–23.
Gorski, L., Matusevich, A., Parzuchowski, P., Luciuk, I., Malinowska, E., 2010. Anal. Chim. Acta 665, 39–46.
Guillen, I., Guardiola, L., Almela, L., Nunez-Delicado, E., Gabaldon, J.A., 2017. Food Anal. Method. 10, 1430–1441.
Guinovart, T., Hernandez-Alonso, D., Adriaenssens, L., Blondeau, P., Rius, F.X., Ballester, P., Andrade, F.J., 2017. Biosens. Bioelectron. 87, 587–592.
Jasielec, J.J., Mousavi, Z., Granholm, K., Sokolski, T., Lewenstam, A., 2018. Anal. Chem. 90, 9644–9649.
Jung, W.E., Han, J., Choi, J.W., Ahn, C.H., 2015. Microelectron. Eng. 132, 46–57.
Lee, C.H., Folz, J., Zhang, W.L., Jo, J., Tan, J.W.Y., Wang, X.D., Kopelman, R., 2017. Anal. Chem. 89 (13674-13674).
Lin, K.Y.A., Liu, Y.T., Chen, S.Y., 2016. J. Colloid Interface Sci. 461, 79–87.
Luppa, P.B., Muller, C., Schlichtiger, A., Schlebusch, H., 2011. Trac-Trend Anal. Chem. 30, 887–898.
Massoudinejad, M., Ghaderpoori, M., Shahsavani, A., Amini, M.M., 2016. J. Mol. Liq. 221, 279–286.
Meenakshi, S., Viswanathan, N., 2007. J. Colloid Interface Sci. 308, 438–450.

Meng, H.M., Liu, H., Kuai, H.L., Peng, R.Z., Mo, L.T., Zhang, X.B., 2016. Chem. Soc. Rev. 45, 2583–2602.
Ortuno, J.A., Garcia, M.S., Albero, M.I., Cuartero, M., 2009. Sens. Lett. 7, 615–620.
Papp, S., Jagerszki, G., Gyurcsanyi, R.E., 2018. Angew. Chem. Int. Ed. 57, 4752–4755.
Qin, L., Zeng, G.M., Lai, C., Huang, D.L., Zhang, C., Xu, P., Hu, T.J., Liu, X.G., Cheng, M., Liu, Y., Hu, L., Zhou, Y.Y., 2017. Sens. Actuators B-Chem. 243, 946–954.
Quinn, A.D., Dixon, D., Meenan, B.J., 2016. Crit. Rev. Clin. Lab. Sci. 53, 1–12.
Rahman, M.M., 2018. Sens. Actuators B-Chem. 264, 84–91.
Ramezani, M., Danesh, N.M., Lavaee, P., Abnous, K., Taghdisi, S.M., 2016. Sens. Actuators B-Chem. 222, 1–7.
Ren, R.R., Cai, G.N., Yu, Z.Z., Tang, D.P., 2018. Sens. Actuators B-Chem. 265, 174–181.
Rodriguez, I., Hardisson, A., Paz, S., Rubio, C., Gutierrez, A.J., Jaudenes, J.R., Burgos, A., Revert, C., 2018. J. Food Compos. Anal. 72, 97–103.
Seo, P.W., Ahmed, I., Jhung, S.H., 2016. Chem. Eng. J. 299, 236–243.
Sharma, A., Istamboulie, G., Hayat, A., Catanante, G., Bhand, S., Marty, J.L., 2017. Sens. Actuators B-Chem. 245, 507–515.
Solangi, I.B., Memon, S., Hanger, M.I., 2009. J. Hazard. Mater. 171, 815–819.
Song, K.M., Cho, M., Jo, H., Min, K., Jeon, S.H., Kim, T., Han, M.S., Ku, J.K., Ban, C., 2011. Anal. Biochem. 415, 175–181.
Song, S.P., Wang, L.H., Li, J., Zhao, J.L., Fan, C.H., 2008. Trac-Trend Anal. Chem. 27, 108–117.
Storhoff, J.J., Elghanian, R., Mucic, R.C., Mirkin, C.A., Letsinger, R.L., 1998. J. Am. Chem. Soc. 120, 1959–1964.
Tang, Y.L., Guan, X.H., Wang, J.M., Gao, N.Y., McPhail, M.R., Chusuei, C.C., 2009. J. Hazard. Mater. 171, 774–779.
Tolle, F., Brandle, G.M., Matzner, D., Mayer, G., 2015. Angew. Chem. Int. Ed. 54, 10971–10974.
Vashist, S.K., Luppa, P.B., Yeo, L.Y., Ozcan, A., Luong, J.H.T., 2015. Trends Biotechnol. 33, 692–705.
Wang, C.S., Liu, C., Luo, J.B., Tian, Y.P., Zhou, N.D., 2016a. Anal. Chim. Acta 936, 75–82.
Wang, L., Wang, E.K., 2004. Electrochem. Commun. 6, 49–54.
Wang, X.Z., Dong, S.S., Gai, P.P., Duan, R., Li, F., 2016b. Biosens. Bioelectron. 82, 49–54.
Yang, L.L., Tao, Y.Z., Yue, G.Y., Li, R.B., Qin, B., Guo, L.H., Lin, Z.Y., Yang, H.H., 2016. Anal. Chem. 88, 5097–5103.
Yang, X., Lv, J.J., Yang, Z.H., Yuan, R., Chai, Y.Q., 2017. Anal. Chem. 89, 11636–11640.
Zdrachek, E., Bakker, E., 2017. Anal. Chem. 89, 13441–13448.
Zhao, X.D., Liu, D.H., Huang, H.L., Zhang, W.J., Yang, Q.Y., Zhong, C.L., 2014. Microporous Mesoporous Mater. 185, 72–78.
Zhou, H.C., Kitagawa, S., 2014. Chem. Soc. Rev. 43, 5415–5418.
Zhou, H.C., Long, J.R., Yaghi, O.M., 2012. Chem. Rev. 112, 673–674.
Zhou, W., Ling, Y., Liu, T., Zhang, Y., Li, J.Z., Li, H.N., Wu, W.J., Jiang, S.J., Feng, F., Yuan, F., Zhang, F., 2017. J. Chromatogr. B 1061, 411–420.